metals

MDPI

Article

Ultrasonic-Assisted Brazing of Titanium Joints Using Al-Si Based Fillers: Numerical and Experimental Process Design

Abdulsalam Muhrat * and Joaquim Barbosa

CMEMS-UMinho, Mechanical Engineering Department, University of Minho, 4800-058 Guimarães, Portugal; kim@dem.uminho.pt

* Correspondence: eng.abdulsalam.edu@gmail.com or id5666@alunos.uminho.pt

Abstract: The ultrasonic-assisted brazing process was studied both numerically and experimentally. The ultrasonic brazing system was modeled by considering the actual brazing conditions. The numerical model showed the distribution of acoustic pressure within the filler and its variations according to the gap distance at different brazing temperatures. In the experimental part, brazing joints were studied and evaluated under multiple conditions and parameters. Although either the initial compression load or the ultrasonic vibration (USV) can initiate the interaction at the interface, the combined effect of both helped to produce joints of a higher quality with a relatively short brazing time, which can be further optimized in terms of their mechanical strength. The effect of the Si content on the joint interface, and the effect of the brazing conditions on the microstructures were studied and discussed.

Keywords: brazing; titanium; aluminum alloys; ultrasonic vibration; acoustic pressure; numerical simulation

Citation: Muhrat, A.; Barbosa, J. Ultrasonic-Assisted Brazing of Titanium Joints Using Al-Si Based Fillers: Numerical and Experimental Process Design. *Metals* **2021**, *11*, 1686. https://doi.org/10.3390/met11111686

Academic Editor: Russell Goodall

Received: 24 September 2021
Accepted: 11 October 2021
Published: 23 October 2021

1. Introduction

The brazing of titanium using aluminum-based filler alloys was investigated previously under a variety of conditions and using multiple filler alloys [1]. The main objectives were the simplification of the experimental conditions, controlling the formation of the intermetallic layer, and developing filler materials in order to achieve the highest possible strength [1–3]. The surface of titanium oxidizes instantly when it is exposed to the ambient air at room temperature. The amorphous and passive oxide film of titanium consists of three layers: the anatase TiO_2 in contact with the surroundings, then Ti_2O_3, and finally TiO which is in contact with the metal Ti. Although the biocompatibility and corrosion resistance of titanium and its alloys are attributed to its surface oxide film [4,5], these oxide layers must be removed or destroyed to establish a metal–metal connection in welding or brazing processes. Therefore, preventing the formation of a thicker oxide layer during the heating phase, followed by destroying the existing layers, is an essential factor in achieving high-quality joints in a short brazing time.

Ultrasonic vibration (USV) is employed in brazing as a tool for assisting in the destruction of the oxide film and in enhancing the joint characteristics [6–8]. Under the impact of the developed cavitation within the liquid filler, the oxide film on the base metal breaks and distributes in the joint. The effect of the ultrasonic vibration in destroying the oxide film was investigated by Chen et al. [7]. The developed cavitation instantly promotes the direct contact between the filler material and the base metal. This fast breakage of the oxide layer is combined with the homogenization of the molten filler, which enhances its spread [7–9]. Usually, and for the above-mentioned reasons, ultrasonic brazing processes are done in the air. However, the application of a single USV process was not enough to remove the oxide film [8]. To improve the interaction at the interface and to remove the floating oxide layer, a relatively long holding time at a liquid filler state and second period

of USV were needed. In this case, the thickness of the intermetallic at the joint interface increased to reach ~5 µm at 620 °C [8].

In an earlier investigation, it was found that adding pressure/compression load/ with the help of the parent metal's surface roughness helped to break the oxide layer of the Al-based filler, whereby the buckling proceeded through-thickness cracking of the oxide layer. The stripped Al surface atoms could then react with the Ti oxide to reduce it to atomic Ti [2]. However, the thickness of the joint was a constant factor that followed the roughness and the applied pressure. Conversely, according to the literature, often after holding the brazing assembly within a certain fixture the changes that could be imposed due to parts expansion were not given proper attention. By applying or introducing an uncontrolled load, an uncertain/uncontrolled amount of filler could be displaced outside the joint upon reaching the brazing temperature. An unexpected loss in the filler material affects the efficiency of the brazing process beyond the alteration of the filler composition due to the liquation of the phases of the low melting points.

In this work, a dedicated brazing equipment supported by a numerical study were presented and employed to control and optimize the parameters of the ultrasonic-assisted brazing process. The work aimed to study the behavior of the filler under the USV and to define the proper joint thickness, including other process parameters such as the effects of a controlled initial compression load and the Si content in the filler.

2. Materials and Methods

2.1. Preparation of Bulk Filler Alloys

The filler alloys used in this study were Al-1Si, Al-13Si, and Al-9Si-3Cu. The Al-1Si was prepared by remelting and degassing the proper portions from the Al-13Si ingot and pure aluminum. The Al-9Si-3Cu and Al-13Si filler alloys were cut from their ingots and degassed. Table 1 shows the measured compositions of the filler alloys. In the preparation of the filler, an electrical resistance furnace equipped with a PID temperature controller was used for the melting processes under a normal air atmosphere. Furthermore, an electric furnace was used for heating the mold. Additional external type K thermocouples and an NI-9211 temperature input module from National Instruments Corporation were used for the temperature readings of the mold and the melt. The process ended with a 10 min degassing by Ar, and then pouring from 720–730 °C in a 200 °C mold. After pouring directly, the mold with the cast was immersed in a tap water container. A part of each alloy was later used to record the cooling curve, followed by calculating the first and the second derivatives. The nonequilibrium liquidus temperatures were determined on the cooling curves (Figure 1). The remelted quantities for recording the cooling curves were not subjected to any further treatment with Ar. The microstructures of the filler alloys Al-9Si-3Cu and Al-13Si are presented in Figure 2.

Table 1. Compositions of the filler alloys using an optical emission spectroscopy (wt.%).

Filler Alloy	Si	Mg	Fe	Cu	Mn	Ti	Zn	Cr	Al
Al-13Si	13.12	0.007	0.47	0.022	0.005	0.012	0.024	0.009	Bal.
Al-1Si	1.042	0.001	0.097	0.006	0.005	0.007	0.015	0.002	Bal.
Al-9Si-3Cu *	9.183	0.178	0.891	3.178	0.253	0.029	0.835	0.043	Bal.

* Al-9Si-3Cu has also (0.072 Pb and 0.017 Sn) wt.%.

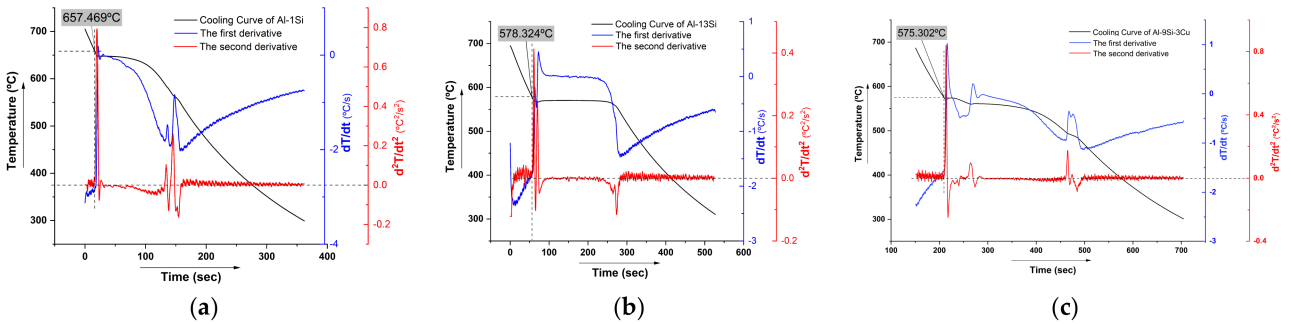

Figure 1. The measured nonequilibrium cooling curves and their first and second derivatives of filler alloys: (**a**) Al-1Si; (**b**) Al-13Si; (**c**)Al-9Si-3Cu, where their compositions are presented in Table 1.

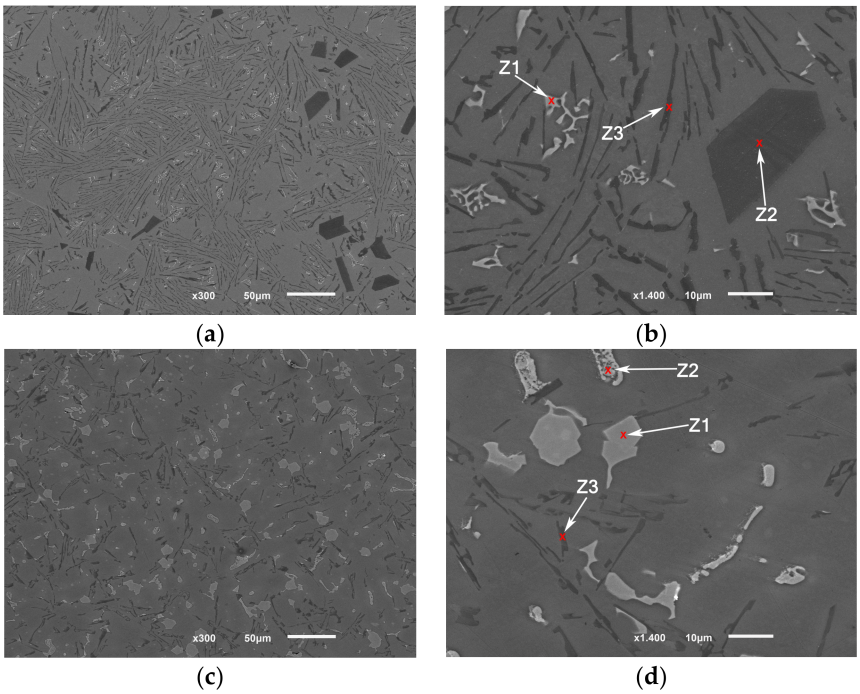

Figure 2. SEM images (SEI) of Al-13Si and Al-9Si-3Cu filler alloys degassed by Argon. All filler alloys were prepared without USV treatment: (**a**,**b**) Al-13Si, where Z1 is a script-like $Al_{15}(Fe,Mn)_3Si_2$, Z2 is primary silicon, and Z3 is eutectic silicon; (**c**,**d**) Al-9Si-3Cu, where Z1 is bulky $Al_{15}(Fe,Mn,Cr)_3Si_2$, Z2 is complex eutectics of Al_2Cu and Al-Cu-Mg-Si (EDS, at.%: Al(67.5%)-Cu(24%)-Si(5.9%)-Mg(2.6%)), and Z3 is eutectic silicon.

2.2. Preparation of the Brazing Assembly

The filler materials were cut and prepared from the degassed casts with a thickness of $0.7^{+0.005}_{-0.025}$ mm and dimensions of 9×22 mm^2 for the majority of the trials, and 12×22 mm^2 for an additional part. The base metals of $118 \times 22 \times 3$ mm^3 were cut from a sheet of titanium (Al-6Al-4V). Prior to the brazing process, the faying surfaces of the parent and the filler materials were ground by successive grinding papers, finishing with P800 for the filler materials, while the base metal was ground only using P100. Grinding was followed by cleaning with alcohol and drying with hot air. The filler materials slices were further cleaned by alcohol in an ultrasonic cleaner for 4 min. The brazing assembly and its detailed dimensions are shown in Figure 3. The "active part" description was given to the base metal part connected to the sonotrode, while the "passive part" to the other part of the base metal.

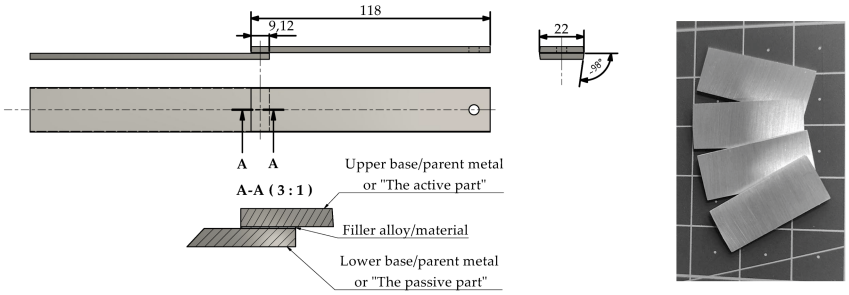

Figure 3. Brazing assembly: (**a**) Brazing assembly components and dimensions (mm), where A–A is the cross-section for the microstructures observation, the examined location during this study is close to the middle of the section A-A if not reported differently; (**b**) The form of the filler materials.

2.3. Fillers and Joints Characterization

The chemical compositions of the filler alloys (Table 1) were determined using SPECTROMAXx optical emission spectroscopy (SPECTRO, AMETEK Materials Analysis Division). For each batch of spectrometer measurements, a standard sample with accurate composition was used for further calibration of the measurements.

After the brazing process, the brazed joints were cut at the middle (approximately 0.5 mm around the center line), as demonstrated in Figure 3a (section A–A). The sectioned samples for the microstructure and chemical analyses were ground using a series of increasingly fine SiC papers up to P4000, and then polished with polycrystalline 1 μm diamond suspension followed by 0.02 μm of colloidal silica. All the samples were ultrasonically cleaned. A light microscope LEICA DM 2500 M (Leica Microsystems) was used for the evaluation of the microstructure and for observing the cleanness of the bulk filler alloys.

An image processing package, ImageJ (National Institutes of Health, Bethesda, MD, USA), [10] was used for any further measurements.

A JSM-6010LV (JEOL, Japan) Scanning Electron Microscope (SEM) equipped with an energy dispersive spectroscope (EDS) (INCAx-act, PentaFET Precision, Oxford Instruments) was used for further microstructure characterization and chemical composition analyses of the phases.

2.4. Experimental Set-Up

A dedicated experimental brazing apparatus was designed and machined (Figure 4). Using this apparatus, the load and temperature were real-time monitored and controlled accurately during the brazing process. Any expansions in the pressing/fixture mechanism's parts during the brazing cycle were detectable and recorded along with the corresponding time and temperature. The brazing assembly was calibrated to a horizontal position. The position of the brazed assembly is adjustable and was calibrated according to the required brazing gap. A special furnace/heating chamber fitted with a PID temperature controller was designed and tuned to deliver high-speed and accurate heating for the brazing assembly at the joining location. The brazing assembly was prepared and placed in the brazing furnace chamber before heating, then an initial load of 20 kg was applied to the assembly using the pressing mechanism (Figure 4a) with two ceramic pivots and two titanium end cups on the opposites ends of the pivots. The sonotrode end was attached to the end of the upper part of the parent metal (the active part) using a 5 mm screw. To guarantee the consistent delivery of the USV to the joint, a torque of 10 Nm delivered by a high precision adjustable torque wrench was applied to the screw. Two type K thermocouples of a special limit of error (0.4%) were used to have better control over the temperature of the brazing process. One of the thermocouples was connected to the PID temperature controller within the dedicated control box, and the other to the NI-9211 temperature input module (National Instruments Corporation) (Figure 4a,b) to record the furnace temperature. The two thermocouples were attached to the lower titanium end cup.

The temperature difference between the fixture and the filler was realized using a third thermocouple that was inserted in the filler itself. A proper and lag-free application using the LabVIEW environment was developed for this purpose. To protect the furnace coils from the liquid metal splashing/sputtering, two thin metallic foils were added to the lower titanium cup around the two sides of the joint (Figure 4c).

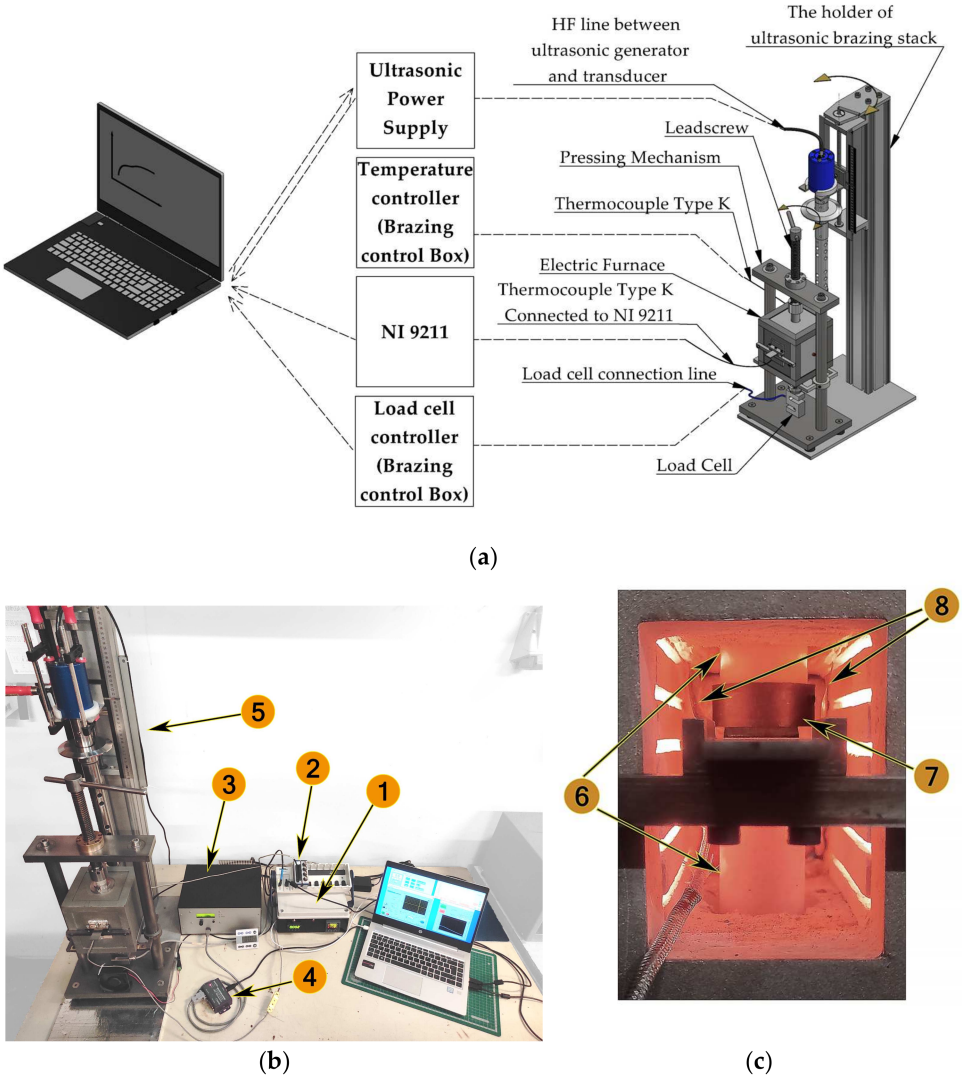

Figure 4. (**a**) Schematic diagram of ultrasonic brazing device showing signal flows between PC and the ultrasonic brazing equipment through the related peripherals; (**b**) The actual equipment assembly including: 1- brazing control box which contains furnace temperature controller and load cell controller, 2- the NI 9211 input module (14 S/s, 4 channels), 3- the ultrasonic power supply (MP Interconsulting, Switzerland), 4- the RS485-USB convertor between ultrasonic power supply and PC, and 5- the ultrasonic brazing stack with holder; (**c**) The position of the sample inside the furnace where: 6- the ceramic pivots, 7- the upper titanium end cup, 8- two thin metallic foils to protect the furnace coils from the liquid metal splashing/sputtering, brazing assembly is enclosed between the upper and the lower ends cups (Further details are shown in Figure 8a). All furnace sides were closed during the operation as it is shown in (b).

The ultrasonic system consisted of a 1000 W ultrasonic power supply (MP Interconsulting, Switzerland), a high-power ultrasonic converter (piezoelectric transducer), an acoustic booster (1:1), a waveguide, and a sonotrode.

The sonotrode was tuned to work at 19.5 ± 0.3 Khz at a work temperature similar to that followed in [11]. The unloaded ultrasonic stack delivers $17 - 20$ μm (P–P) at its free

end at a normal temperature (without attaching the active part of the base metal). Two to three seconds were needed to reach the defined amplitude from the start of the ultrasonic generator (ultrasonic power supply).

2.5. Brazing Methods and Conditions

Titanium brazing using aluminum filler alloys is normally accompanied by the formation of Al_xTi_n intermetallic compounds at the interface. The formation of those intermetallic compounds depends on the brazing temperature, the alloying elements in the filler materials, and the composition of the parent material. Adding the USV results in further complications for the process. To evaluate the effects of the Si addition, USV, and initial load, the brazing cycle presented in Figure 5 and the related parameters in Table 2 were followed.

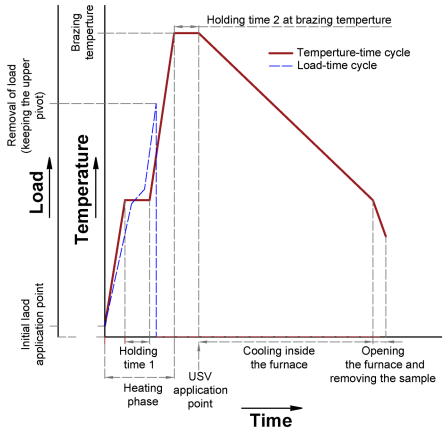

Figure 5. Brazing cycle using the parameters presented in Table 2. The diagram shows a sketch of the observed load changes due to expansion. After application of the primary load of 20 kg, the load increase due to the expansion was removed after passing the solidus temperature of the filler at the point N2 (explained in Section 3.2) to prevent any displacement of the filler before reaching the USV application point. The temperature-time cycle represents the cycle applied by the furnace controller, actual recorded cycles will be presented later in this work. All holding times started −5 °C to the required temperature. The brazed joint was cooled inside the furnace. During cooling, furnace sides were removed at 300 °C. The sample was removed from the furnace after the cooling temperature passed 250 °C.

Table 2. Brazing trials parameters which were used in the brazing cycle presented in Figure 5.

Condition Code	Filler Type	Initial Load (kg)	Holding 1 Temperature/Time (°C/min)	Holding 2 at Brazing Temperature/ Time (°C/min)	USV Period, (Sec) -Furnace off-
13/680	Al-13 Si	20	300/3	680/3	10
1/680	Al-1 Si	20	300/3	680/3	10
13/585	Al-13 Si	20	300/3	585/3	10
13/585L	Al-13 Si	20	300/3	585/3	-
13/585U	Al-13 Si	-	300/3	585/3	10
9-3/580	Al-9Si-3Cu	20	300/3	580/3	10

2.6. Numerical Modeling

To investigate the distribution of the acoustic pressure in the filler and its variations against the gap distance and temperature, a numerical model was studied using COMSOL Multiphysics® [12]. The simulation solution presented the effect of the gap distance and

temperature on the efficiency of the ultrasonic process through the acoustic pressure. A geometrical representation of the studied system is presented in Figure 6.

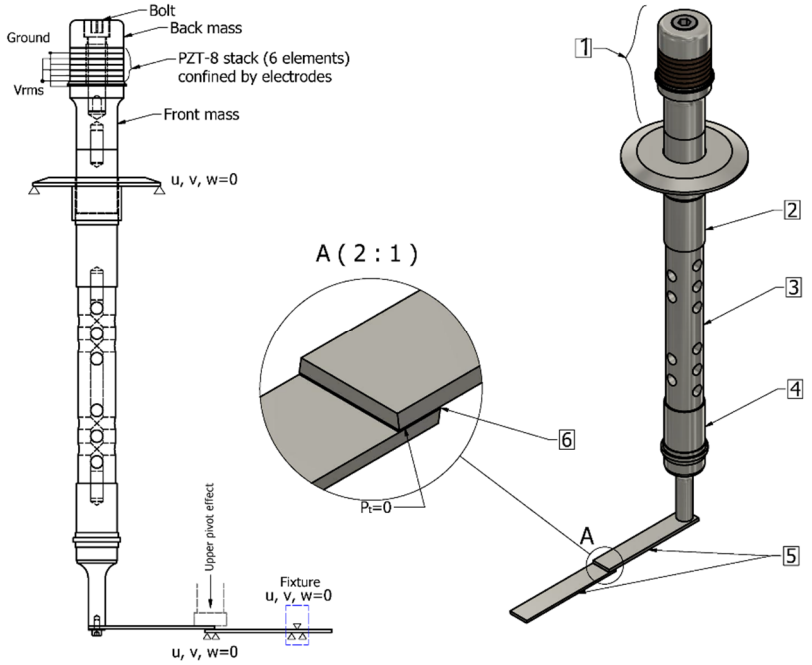

Figure 6. The studied ultrasonic brazing stack with a 20 kHz transducer (Ti-6Al-4V front mass): (1) transducer of 6 elements PZT-8, Ti-6Al-4V front mass; (2) 1:1 booster; (3) waveguide; (4) sonotrode; (5) the base metal parts where the active part is connected to the sonotrode; (6) filler alloy of Al-13Si.

The model was solved in the frequency domain as a coupled acoustic–piezoelectric structure analysis. The temperature distribution in the brazing assembly and the ultrasonic stack was measured during the experiment and then coupled to the simulation model through the heat transfer model.

The flow of the molten filler was assumed to be lossless and adiabatic, and viscous effects were neglected. The frequency domain formulation uses a reduced wave equation to the Helmholtz equation [13,14]:

$$\frac{\omega^2 p}{\rho_0 \alpha^2} = \nabla . \left(-\frac{1}{\rho_0} \nabla p \right) \tag{1}$$

where ρ_0 is the fluid density in kg/m^2, p is the pressure in Pa, ω is the angular frequency in rad/s, and α is the speed of sound in the fluid in m/s. At the interface between the filler and the base metal, the model node used the fluid pressure and the structural acceleration as a bidirectional coupling.

The solid mechanics and electrostatics physics interfaces were used to model the piezoelectric effect of the Langevin type transducer, of the mode 33. The piezoelectric effect was modeled by coupling the stresses and strains with the electric field and the electric displacement via linear constitutive equations. In terms of the piezoelectric stress coefficient matrix T, the mechanical and electrical behaviors are defined by [14,15]:

$$\begin{aligned} T &= c_E S - e^T E \\ D &= eS + \epsilon_0 \epsilon_{rS} E \end{aligned} \tag{2}$$

where S is the strain tensor, T is the mechanical stress tensor, E is the electric field, and D is the electric displacement field. The material parameters c_E, e, ϵ_{rS}, and ϵ_0 correspond to the material's elastic stiffness matrix (Pa), coupling matrix (C/m^2), relative permittivity at constant strain, and the vacuum permittivity. The unloaded transducer was studied

considering both the 0.001 damping factor and 0.002 coupling factor. Adding the other components of the ultrasonic stack, temperature changes during the operation, and any additional loading will change the damping characteristics of the system.

The results were calculated at multiple gap distances. Due to heating, the extension of the lower pivot affects the position of the passive part at the joint area. In the studied system (Figure 6), the expansion of the lower pivot was not considered in order to be subtracted later from the initial joint gap according to its value at the brazing temperature. The relative positions of the brazing assembly components can be configured to achieve later at brazing temperature the required gap between the faying surfaces of the joint.

During the ultrasonic brazing, the joining area was under a slight weight of the unfixed upper pivot (110 g) (Figure 4c). The effect of the free upper pivot was added to the damping input in addition to its prestress effect on the active part. In the simulation model, the ultrasonic stack was fixed from a nodal location on an attached part (of steel) to the booster (Figure 6) instead of the transducer housing (Figure 4a,b). The main parts (i.e., sonotrode, waveguide, and booster) were made of Ti-6Al-4V alloy. Two brazing temperatures at 680 and 585 °C, respectively, were studied for the Al-13Si filler alloy.

3. Results and Discussion

3.1. The Numerical Results

Having a clear understanding of the distribution of vibration amplitude and the acoustic pressure is essential for achieving high-quality joints and avoiding some of the possible defects during the process. The interaction at the interfaces, the refining, and the displacement of the filler are influenced by the amplitude and the developed acoustic pressure in the joint area.

The frequency sweeping and eigenfrequency analyses were applied to the studied system. The converter's (transducer) frequency range between the parallel f_{p1} and series f_{s1} frequencies must contain the stack operational frequency. The operational frequency range of the stack may be anywhere between the converter f_{s1} and f_{p1}, preferably close to f_{s1}; however, the temperature changes during the operation should also be considered.

Figure 7a shows the impedance curves for the studied transducer only and after adding to the transducer the other ultrasonic stack components (booster + waveguide + sonotrode) and the base metal (the active part only) at room temperature. At elevated temperatures, the physical properties of the ultrasonic stack and the base metal change, adding to that the filler in contact with the active base metal which is under the slight weight of the upper pivot. As a result, the operating frequency decreased as well as the damping of the system increased.

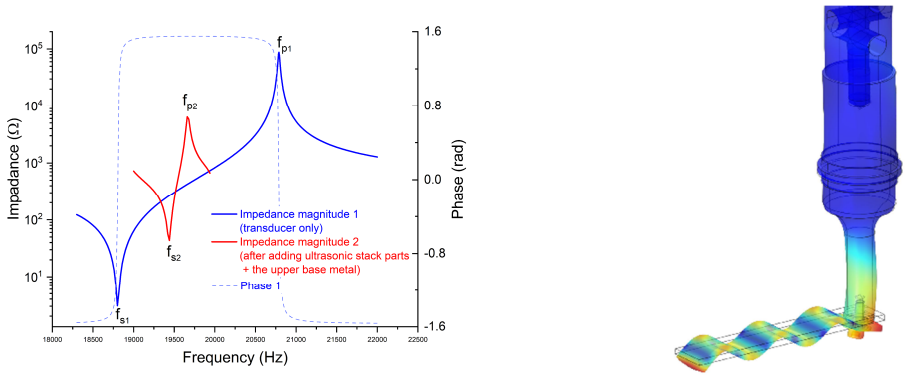

(**a**) (**b**)

Figure 7. (**a**) Electrical impedance magnitude and phase of the transducer as a function of the frequency: transducer only (1) and after adding the other ultrasonic stack components with the base metal /the active part only (2); (**b**) The vibration mode (unitless) of the attached base metal (in the air at normal temperature).

The longitudinal vibration in the ultrasonic mechanical system was transformed into a transverse vibration mode of the connected parent metal (Figure 7b).

To correctly represent the effect of heat variations on the system behavior, this study included the actual temperature distribution measured through similar brazing conditions. Thermocouples were attached to three locations (2, 3, and 4 in Figure 8a,c) in addition to the furnace thermocouple (1a in Figure 8a,c), and then an assistant heat transfer module was used to represent the temperature distributions prior to the activation of the USV and coupled to the studied case (Figure 8).

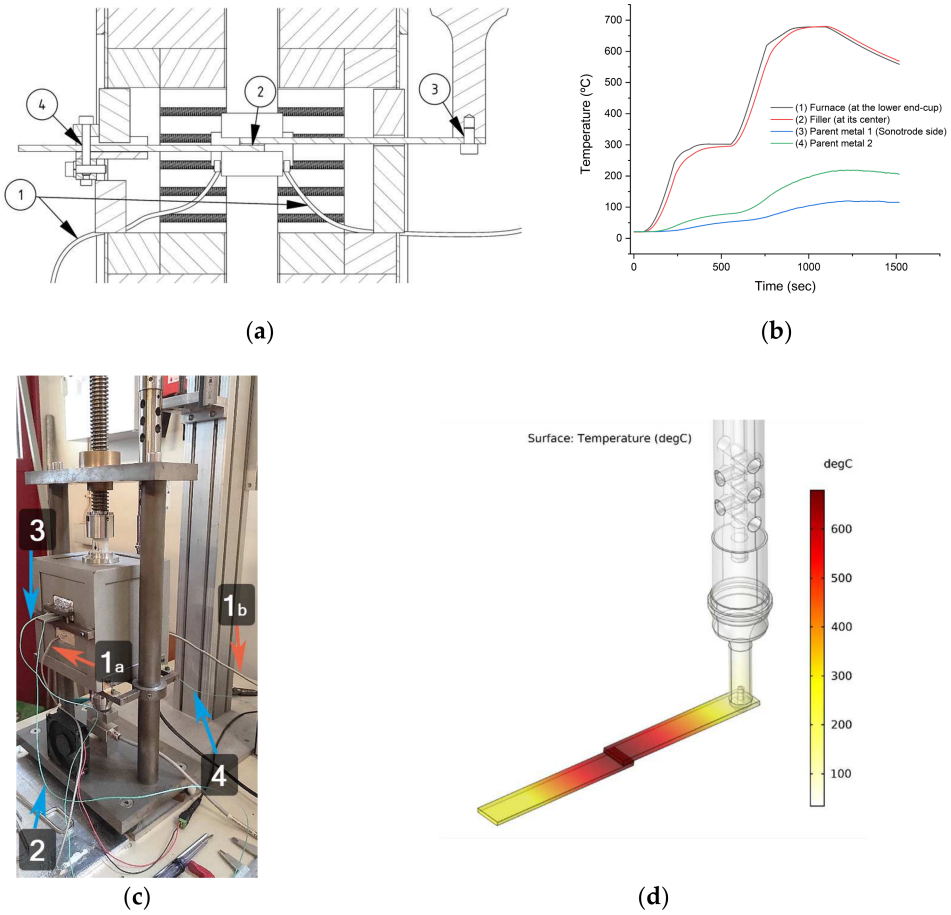

Figure 8. (**a**,**c**) The thermocouples locations during the brazing process at 680 °C; (**b**) The recorded temperature changes vs. time in the locations marked in (a) and (c); (**d**) Temperature distribution prior to brazing measured using Al-Si-Cu based filler. Due to the small thickness and mass of the filler compared with other components, the curve in (b) can be used, at brazing temperature, with a very good approximation for other Al-Si based fillers of close melting ranges. For the lower temperature (585 °C), an actual recorded time- temperatures curves for filler/furnace were used, while the other temperatures in the locations (3) and (4) can be approximated and calculated using the recorded curves in (b) by considering the similarity of the temperature controller characteristics and the brazing conditions.

Due to the significant tendency of the intermetallic layer formation between the aluminum-based fillers and the titanium-based parent metal, the furnace and its controller were carefully designed and tuned as it was mentioned before. Figure 8b shows the difference between the measured furnace and filler temperatures during the heating phase. In the current setup, a 3 min holding time was enough to reach the designated brazing temperature in the filler. The filler temperature in Figure 8b was measured using type K thermocouple, Ø 0.13 mm, of special error range (0.4%). The thermocouple was inserted in

the filler where the measured length was about 4 mm along the middle section line (A–A) (in Figure 3a) within the filler.

Figure 9 shows the vibration mode and its amplitude during the brazing process, and the effect of the gap distance vs the acoustic pressure.

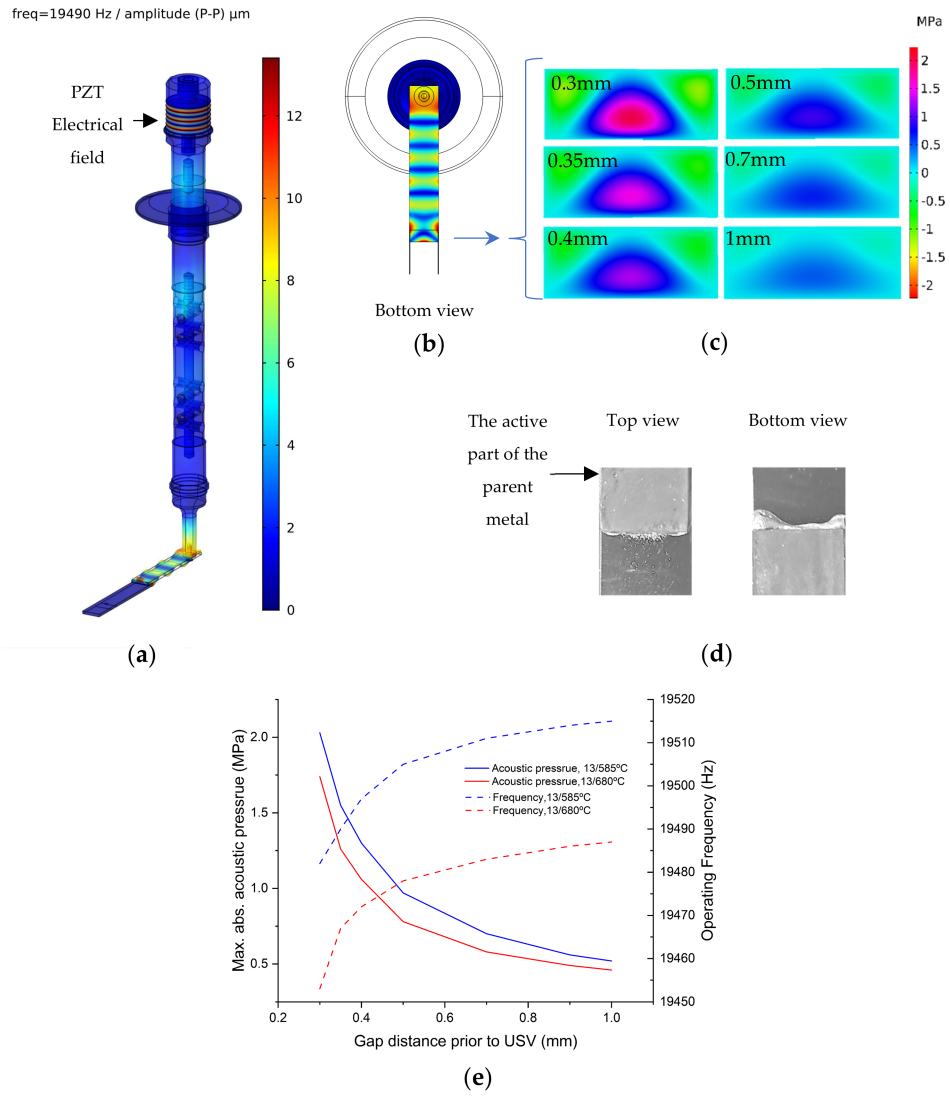

Figure 9. (**a**) The displacement obtained for the system during brazing process (0.35 mm thickness of the filler Al-13Si at 585 °C); (**b**) Bottom view of the active part of the parent metal with the same scale legend of (a); (**c**) The acoustic pressure distribution at brazing temperature 585 °C in the filler of different thicknesses—bottom view; (**d**) Typical joint of Al-13Si brazed at 585 °C, confirming the filler behavior according to the vibration mode and acoustic pressure distribution; (**e**) Filler thickness (gap distance) vs acoustic pressure and operating frequency (±3 Hz)at 680 and 585 °C brazing temperatures.

The gap distance and the acoustic pressure have an inverse relationship, and as can be observed from the results (Figure 9e), the max acoustic pressure value at 0.7 mm is around 0.6–0.7 MPa which increases to around 1.7–2 MPa at a 0.3 mm gap distance (the higher is for the lower brazing temperature of 585 °C). The logical inverse relationship characterized in this simulation model is in accordance with the practical observations of [16]. In the treatment of the bulk aluminum alloy melt, the measured cavitation threshold is around 1 MPa of acoustic pressure. This value was measured at a temperature close to the melting point for Al-Mg alloys and at a slightly higher temperature for the Al-17Si alloy. Increasing

the temperature decreases the cavitation threshold to reach, e.g., 0.8 MPa in Al-6Mg alloy at 700 °C. The cavitation threshold can also be decreased by decreasing the surface tension, which can be achieved by alloying additions such as Mg and Zr [17]. In filler materials the volume quantity of the introduced oxides to the melt is higher than in the bulk case; therefore, a further reduction in cavitation threshold is to be expected. As a result, for the current brazing process, choosing a brazing gap between 0.4–0.3 mm should be enough to obtain good ultrasonic effect. To achieve this gap distance, brazing at a lower temperature (580–585 °C) could be done without compensating the position of the lower base metal, since the expansion of the lower ceramic pivot is around 300–330 μm; however, for the higher brazing temperatures, the compensating should be considered.

Once the filler material becomes fully liquid, regardless of the expansion of the lower pivot, the remaining quantity of the filler within the joint will depend on the balance between the surface tension of the filler in its environment and the slight load at the top of the filler, including the roughness of the base metal surfaces. Under the ultrasonic vibration, the filler materials will show some displacement and splashing/sputtering around the joint sides following the vibration mode and the acoustic pressure. On the active part, a displacement following the vibration mode of the plate was observed, while on the passive part of the base metal a sputtering of the filler was observed, which was generally concentrated around the center line of the joint (Figure 9d). These observations are in accordance with the presented numerical results in this work. It is worth mentioning that the delivered amplitude and the designed gap distance should be selected by taking into account the effective treatment while avoiding an unacceptable level of displacement and sputtering around the joint, which was also considered in this work.

If the expansion of the fixture (the pivots in the current study) is not taken into consideration, the brazing could result in uncontrolled joint thickness and intermetallic formation, as is presented in Figure 10 for a preliminary trial. The large intermetallic particles of Al_3Ti at the lower side of the joint are due to the filler saturation by the dissolved Ti from the parent metal during the USV.

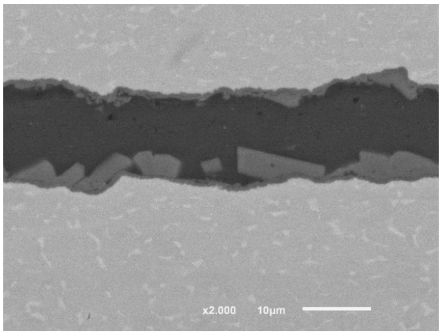

Figure 10. SEM images (BSE) of Ti/Al-1Si/Ti ultrasonic-assisted brazed joint at 665–670 °C without holding time. The intermetallic formation and precipitation of $TiAl_3$ increased due to the very small gap distance between the faying surfaces of the joint.

In the brazing processes, the gap distance between the parent metal parts plays an important role in filling the joint under the capillary force, and later the joint strength will be affected by the resulting joint thickness. In the ultrasonic-assisted brazing process, the joint gap has a further role in controlling the efficiency of the ultrasonic process. The gap distance should be optimized in order to provide adequate acoustic pressure at a specific combination of the ultrasonic power and the materials.

3.2. The Effect of the Initial Compression Load

Due to the heating, the ceramic pivots and other metallic objects, which are in contact with the brazing assembly, start to expand. This expansion leads to an increase in the compression load on the joint during the heating phase, which could lead to a separa-

tion/uncontrolled liquidation of the phases of the low melting points in the filler. Therefore, in most cases, and according to the process design, once the filler reaches its melting point the load on the joint should be removed or reduced and maintained within the limits that do not lead to filler loss from the joint area. Conversely, to reduce the oxidation of the faying surfaces during the heating phase, the assembly surfaces should be kept tight against the surrounding air with a certain amount of the compression load. Given the above-mentioned reasons, applying and controlling the compression load during the heating phase was one of the design concerns in the current study.

To examine the effect of the initial load, the load and temperature changes with time were recorded (until 665 °C) without brazing assembly and then the load–temperature curve was extracted and compared with similar ones of actual brazing processes. All the processes were started by 20 kg initial load application. Without the brazing assembly, the rate of the load increase was high and reached a value around 500 kg according to the cycle presented in Figure 11a. Figure 11b shows a comparison until around 500 °C between two brazing processes and the case without brazing assembly. With the brazing assembly, for example Figure 11c, the load increased with temperature increase until reaching a point where it started to decrease. Before this point no visual displacement of the filler was observed outside the joint, although the increasing rate was decelerating compared to the case without the brazing assembly. After this change point (N1 on Figure 11c) the load was removed (at N2 on Figure 11c) and the assembly was only kept under the slight weight of the upper pivot.

In Figure 11a–c, the recoded temperature is the furnace temperature (the thermocouple attached to the lower end-cup). The filler (Al-9Si-3Cu) temperature at N1 in Figure 11c can be found by recording the filler temperature with furnace temperature at the same time (Figure 11d). According to the heating rate, the size of the sample, and the applied loading, the defined changes by filler's cooling curve may not happen at the expected temperature during heating.

In Figure 11b, the lower measured load values in (1/680 and 9-3/580) comparing with the case without brazing assembly at the same temperature imply that the tightness between the faying surfaces of the joints increases as the temperature increases, where the filler complies under the load and the roughness of the base metal. The rate of the load change with time depends on the properties of the filler, the faying surface preparation, and other parameters which are beyond the scope of the current work. However, the most pronounced effect (i.e., the fast load drop) appears once the filler temperature passes the point N_1. No adjustment was made to reduce the load during the heating process until it reached the previously mentioned point. The purpose was to avoid any relative movements between the assembly components, which avoids a valid comparison among the results. Applying and controlling the initial load on the joint protects the faying surfaces and prevents any uncontrolled rejection of the filler outside the joint before reaching the brazing temperature. By examining the brazed joints close to the middle of the cross section A-A (Figure 3), in the ultrasonic brazed samples without the initial load, after the USV treatment (10 s) the interface showed intermittent interactions (Figure 12a). While in the joints brazed under initial load only, the interface showed continuous interaction (Figure 12b). Under the USV, the dissolution at the parent metal is initiated by the opening of microchannels [7] followed by the formation of the pits (Figure 13). The application of the initial load prevents the severe oxidation of the faying surfaces and facilitates the interaction at the interface. However, in the joints brazed without USV (only by initial load), some voids were still observed at the interface at the joint's sides. In addition, the microstructures showed many bulky silicon particles that were distributed inhomogeneously (Figure 14).

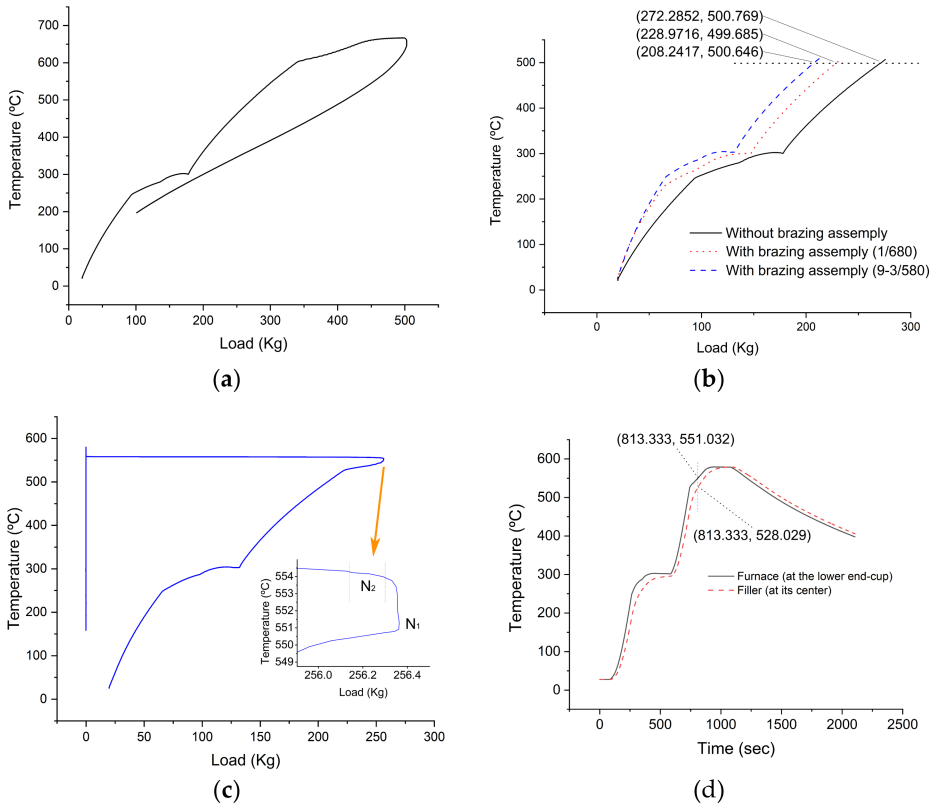

Figure 11. (**a**) A load temperature cycle/3 min holding at 300 °C, 3 min holding at 665 °C/without brazing assembly, the curve is showing the expansion of the ceramic pivots ended by the titanium cups under the effect of temperature, the initial load was set to 20 kg; (**b**) Comparison of load temperature cycles until around 500 °C between two brazing processes and the case in (a), the difference in the load increase rates is an indication of the filler compliance under the load and the roughness of the base metal; (**c**) Load–temperature cycle for brazing process 9-3/580, the load was removed at N_2 after the filler passed the point N_1; (**d**) Actual temperature-time cycles (thermal cycles) of the furnace and the filler Al-9Si-3Cu without USV. The filler temperature in Figure 11d was measured using type K thermocouple, Ø 0.25 mm, of special error range (0.4%).

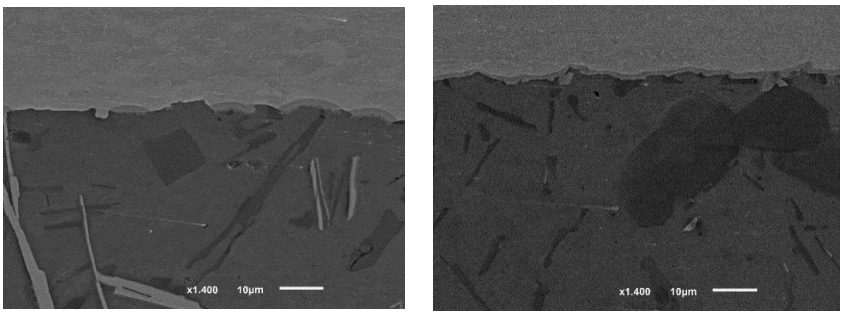

Figure 12. SEM images (SEI) of brazed joints using Al-13Si filler alloy at 585 °C (close to the middle of the joint) where: (**a**) Joint brazed with USV only, "No initial load" (13/585U); (**b**) Joint brazed with initial load only "No USV" (13/585L).

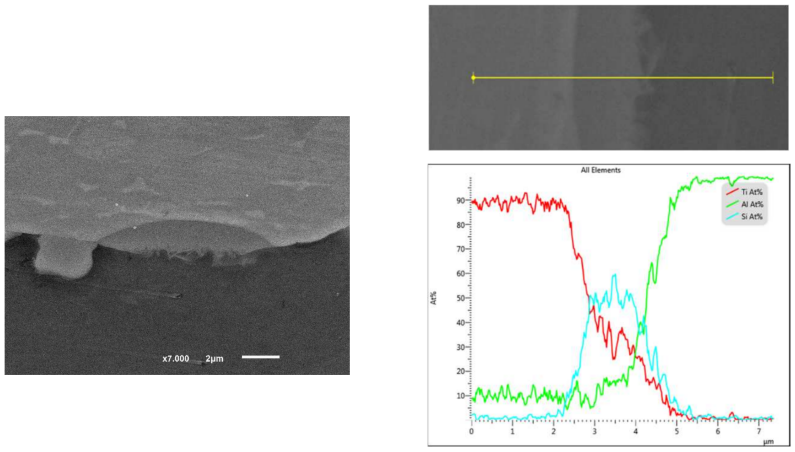

(**a**) (**b**)

Figure 13. (**a**) SEM image (SEI) of a single pit at the joint interface with the active part, using Al-13Si filler alloy at 585 °C, brazed with USV only (13/585U); (**b**) EDS line analysis across the pit.

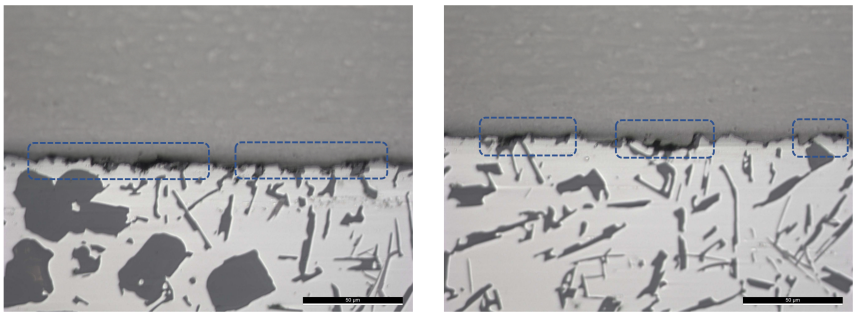

(**a**) (**b**)

Figure 14. Light microscope images of (13/585L) brazed joint using Al-13Si filler alloy at 585 °C with initial load only, "No USV"; close to the joint edge where (**a**) is closer than (**b**). The scale is 50 µm on the images.

The joints brazed under both conditions: the initial load and the USV showed more consistent reaction at the joint interfaces and better joint quality (Figure 15).

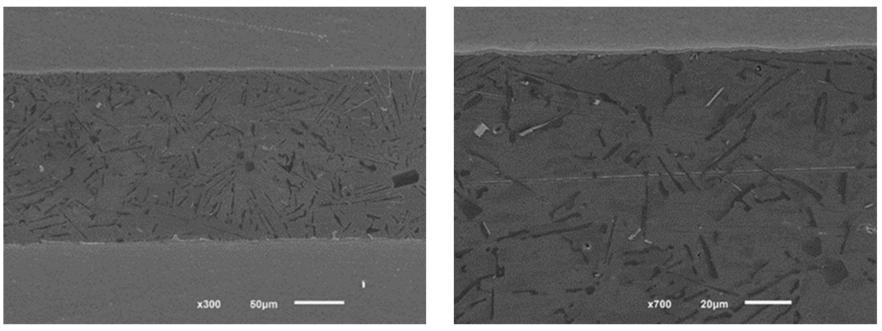

(**a**) (**b**)

Figure 15. (**a**) SEM images (SEI) of brazed joint using Al-13Si filler alloy at 585 °C (13/585) close to the middle of the joint; (**b**) The interface at the active part of the parent metal.

Generally, the thickness of the intermetallic layer at the interface in the brazed joint (13/585L) was the highest around the middle position of the joint (at the cross-section A-A in Figure 3). The middle part of the joint would be more protected from oxidation when comparing it with the edges taking into account the contrived roughness of the joint surfaces prior to assembly. In the joints brazed with the USV, the pit formation intensity

would be higher on the area where the acoustic pressure exceeded the cavitation threshold, as seen in Figure 9c. However, with the assistance of the USV for 10 s, the interfaces were free from the voids and had good visual contact with the base metal. Therefore, combining the initial load and the USV produced, within a short brazing time, joints with higher quality and better interaction at the interface, which can be further optimized in terms of their mechanical strength. The distribution of the intermetallic at the interfaces is affected by both the USV (Figure 9b,c) and the initial load as well as the brazing conditions, and varies along the interface. In most studies, the exact location of the examined area along the cross section was not reported clearly, or the intermetallic evaluation was not presented clearly at the edge of the joints [9,18–26]. However, in the current work conditions, which included the brazing in the air, using the USV, and introducing roughness to the faying surfaces, it was interesting to examine the interface interaction along the entire cross section A–A (Figure 16).

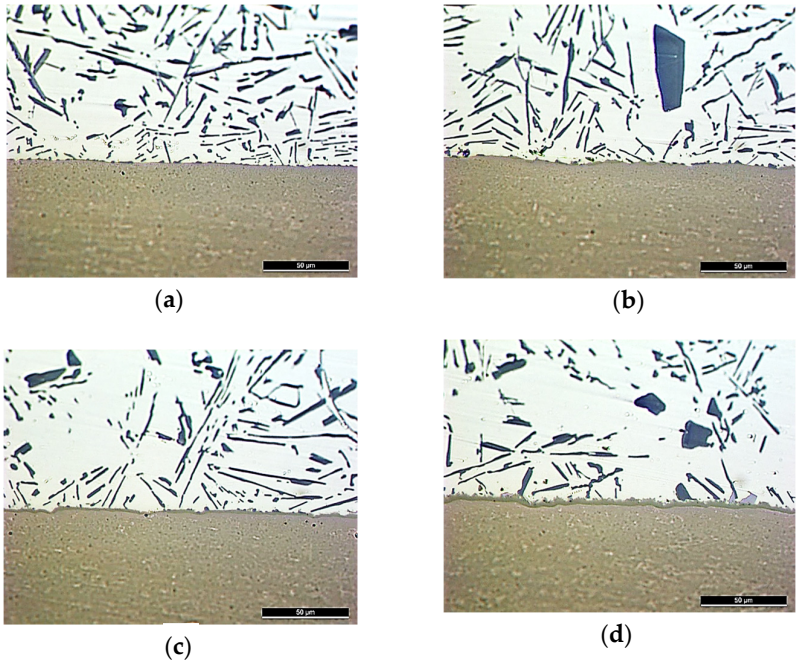

Figure 16. Light microscope images of a brazed joint (13/585) with both initial load + USV, where (**a**) to (**d**) are from a point close to the edge to the highest thickness of the intermetallic at the interface.

When brazing is conducted in the air, ultrasonic vibration has the ability to destroy the oxide layer at joint interfaces and initiate the interaction between the filler and the base metal. For a complete reaction at the interface, usually holding time and/or another USV period are required. However, to reduce the time needed for achieving a better reaction at the interface, and at the same time obtaining a joint with a high quality, an initial compression load can be combined with the USV treatment.

3.3. The Effect of Si and Cu Additions on the Interface

Although the acoustic pressure has higher values at 585 °C when compared to 680 °C, which means a higher impact on the interface, the higher temperature has significant effect on the interaction and the intermetallic formation. The molten aluminium is very active with titanium, causing a high level of erosion which particularly affects the reliability of the thin wall joints. Almost any small additions of alloying elements to the pure Al filler reduces the thickness of the intermetallic layer formed at the interface with the titanium [25]. It was found that the most effective element for suppressing the intermetallic Al_3Ti growth is Si, which could also help develop further intermetallic compounds at the interface. Following that, Si provides the brazing conditions with more flexibility; for instance, the produced

Ti/Al joints using the Al-0.8Si filler exhibited higher joint strengths when compared with the pure Al (as a filler) in relatively higher temperatures and over a wider brazing time window [25]. For brazing conditions at 680 °C for 3 min (the temperature mentioned in the text of [25] was considered), the addition of 3% or more of Si produced a larger thickness of the intermetallic compounds at the interface when compared with an Si addition of 0.8% [25]. However, the alloys have different melting temperatures and thus different contact times between the parent metal and the fully liquid filler during the heating phase until they reach the brazing temperature of 680 °C. Moreover, the joints were brazed in a vacuum environment. Therefore, further investigation at the current brazing conditions is required.

For the sake of comparison, the fillers Al-13Si and Al-1Si were used in brazing at the same temperature (680 °C) and then Al-13Si was used in brazing at a temperature close to its liquidus temperature, which was defined on the recorded cooling curve (Figure 1). When the Al-13Si and Al-1Si fillers were used in brazing at similar elevated temperatures (680 °C), the interfaces with the filler of a higher percent of Si showed an average thickness of 7.4 $\pm$ 0.17 μm (averaged from both joint interfaces and close to the middle of the joint). The observed interface consisted of a dense intermetallic layer followed by a one of scattered laminar morphology (Figure 17). It was proposed that the layers consisted of $Ti_7Al_5Si_{12}$. On the other hand, the interfaces resulted from the interaction of Al-1Si filler alloy with the base metal, composed of two intermetallic layers: a base intermetallic layer with bulky intermetallic particles attached, which formed a second layer (Figure 18) with an average total thickness of 2 $\pm$ 0.3 μm. Examining the EDS line presented in Figure 18, and additional individual EDS points analyses, it was suggested that the outer layer consists of Al_3Ti with an average composition of 72.8 Al, 22.35 Ti, 4.35 Si, and 0.45 V (at.%), and that the base layer next to the parent metal consists of $Ti_9(Al,Si)_{23}$ with an average composition of 59.4 Al, 32.15 Ti, 6.95 Si, and 1.5 V (at.%). The total thicknesses of the intermetallic layers at the interfaces in Al-13Si and Al-1Si were, to some extent, comparable with the work of [25] taking into account some variations such as the brazing method and the compositions of the base metal and filler.

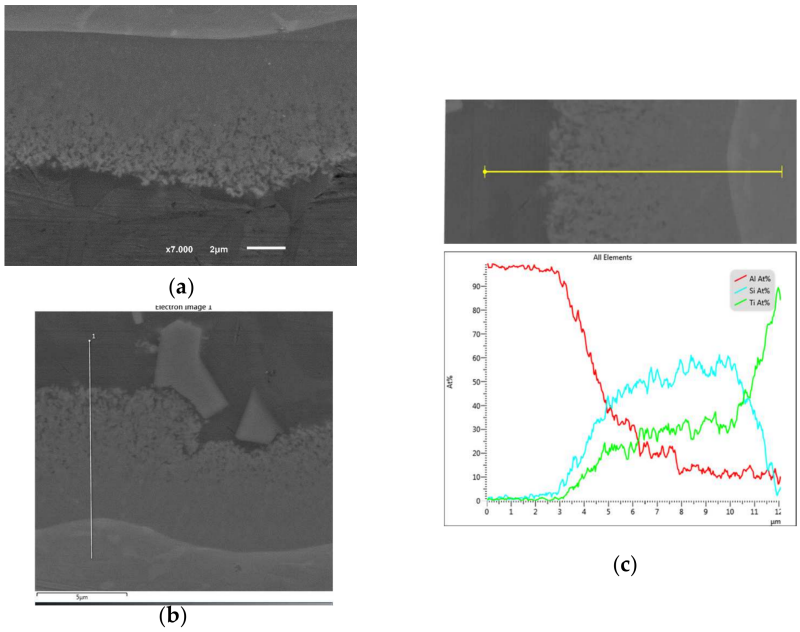

Figure 17. SEM images (SEI) of 13/680 joint interfaces at: (**a**) The active part of the parent metal; (**b**) The passive part; (**c**) EDS line position and analysis of the interface in (**b**). The interfaces show tiny laminar morphology of $Ti_7Al_5Si_{12}$ at the filler side.

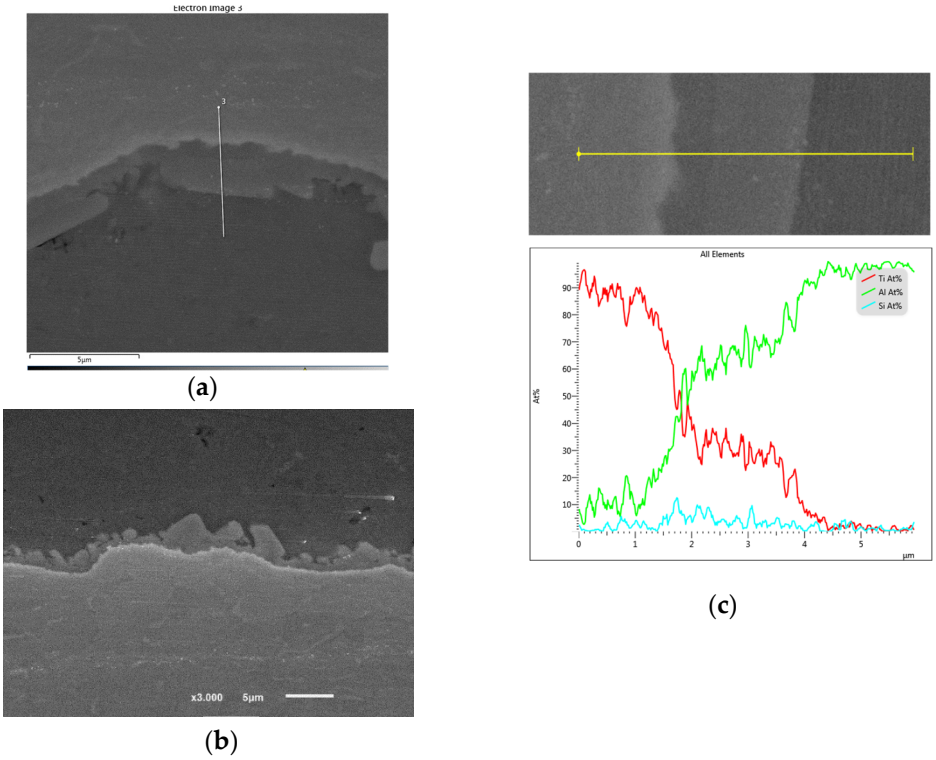

Figure 18. SEM images (SEI) of 1/680 joint interfaces at: (**a**) The active part of the parent metal; (**b**) The passive part; (**c**) EDS line position and analysis of the interface in (**a**).

The brazing using the Al-13Si filler at a lower temperature (585 °C), resulted in an intermetallic thickness of about 1.85 ± 0.1 µm (Figures 19 and 24), which is comparable with the Al-1Si layer thickness at 680 °C, except that the intermetallic layer in Ti/Al-13Si/Ti has a relatively consistent thickness and is composed of $Ti_7Al_5Si_{12}$.

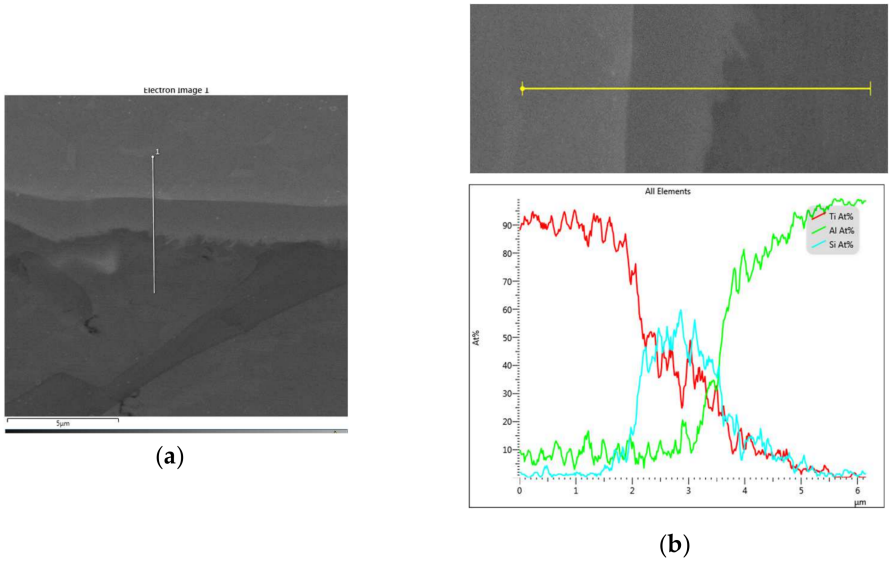

Figure 19. (**a**) SEM images (SEI) of 13/585 joint interface at the active part; (**b**) EDS line position and analysis of the interface in (**a**).

Brazing at a high temperature of 680 °C increases the dissolving rate of titanium into the filler and the diffusion of Si to the interface. In addition, the prolonged contact with the filler in a liquid state during the heating phase, in the case of Al-13Si, contributes to further intermetallic growth when using Al-13Si at a high temperature.

Brazing using Al-9Si-3Cu filler alloy at 580 °C with a similar offset to the liquidus line when compared with the Al-13Si brazed at 585 °C, resulted in a thickness of the intermetallic layer 1.64 ± 0.2 µm that is close to Al-13Si/585 °C, The intermetallic layer was ended in some locations by Cu at the filler side (Figure 20).

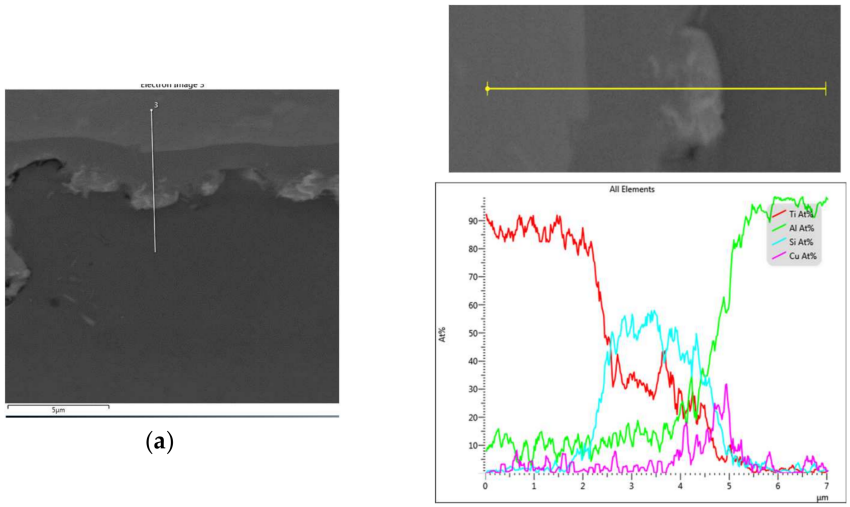

(**a**) (**b**)

Figure 20. (**a**) SEM images (SEI) of a brazed joint (9-3/580) at the active part interface with the filler; (**b**) EDS line position and analysis of the interface in (**a**).

For the higher percent of Si in the filler alloys (Al-13Si and Al-9Si-3Cu), the intermetallic phase that appeared in both sides of the interface was $Ti_7Al_5Si_{12}$. The $Ti_7Al_5Si_{12}$ of a tetragonal crystal structure was reported to have a general formula of $(Ti_{1-x}Al_x)(Al_ySi_{1-y})_2$ with $x \leq 0.12$ and $0.06 \leq y \leq 0.25$. The $Ti_7Al_5Si_{12}$ exists in a composition range from 8 to 20 (at.%) of Al and from 50 to 62.6 (at.%) of Si [27].

The turbulence induced by acoustic streaming promotes Si atom diffusion rate into the pit region. The segregated Si atoms can cause a phase transformation via the following equation [7]:

$$TiAl_3 + 2Al + 6Ti + 12Si \rightarrow Ti_7Al_5Si_{12} \quad (3)$$

The formation of the intermetallic $Ti_7Al_5Si_{12}$ largely reduces the diffusion between Al and Ti, and when its thickness reaches a critical value the mentioned diffusion ceases. It was reported that using Al-Cu filler mainly promoted $TiAl_3$ and a small quantity of Ti_8CuAl_{23} which was difficult to distinguish from Ti_9Al_{23}, in addition, $Cu{>}Al_2$ was detected at the interface [25], however, by the existing of Si, the formation of $Ti_7Al_5Si_{12}$ was dominant over $TiAl_3$. Figure 21 shows the average measured thicknesses of the intermetallic at the joints interfaces and close to the middle of the joints.

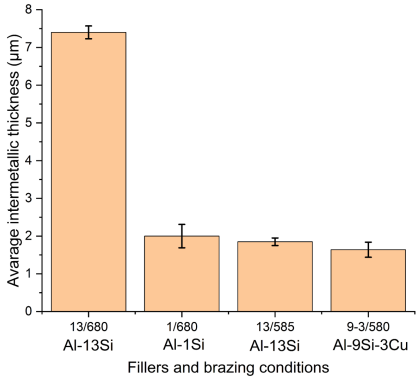

Figure 21. Average intermetallic thicknesses with their standard error at the interfaces of the brazed joints (close to the middle of the joints).

3.4. The Intermetallic Compounds and Silicon within the Joints

Some $Ti_7Al_5Si_{12}$ particles adjacent to the interface were found when the brazing had been done under the initial load only, as with point Z1 in Figure 22. Due to the contrived roughness of the parent metal and the brazing conditions (the initial load), it is possible to expect the formation of some intermetallic particles adjacent to the interface of the joint as a result of the oxide scale cracking and the ensuing reaction between the Al and Ti-oxide layer [2]. During the activation of the ultrasonic vibration, the dissolution of titanium into the filler melt is accelerated and the Ti-intermetallic compounds which form at the interface can separate and enter the joint, as with Z2 and other similar particles in Figure 23b (the EDS analysis is shown in Table 3).

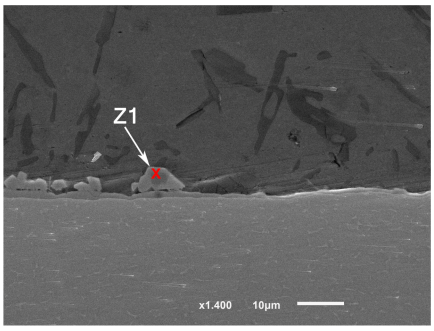

Figure 22. SEM image (SEI) for the joint 13/585L where Z1 is $Ti_7Al_5Si_{12}$.

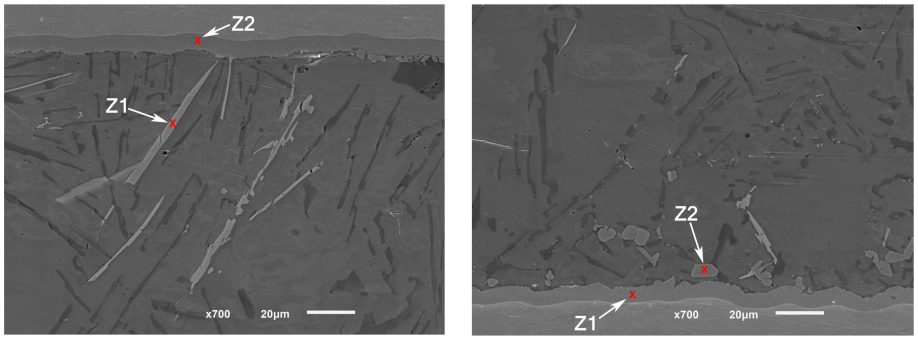

(**a**) (**b**)

Figure 23. SEM images (SEI) of a 13/680 brazed joint: (**a**) The active parent part interface with the filler; (**b**) The passive part interface. EDS analyses results are shown in Table 3.

Table 3. EDS points analyses for the joint 13/680 presented in Figure 23.

	Element:	Al	Si	Fe	Ti	V	Mn	Estimated Main Phase(s)
		at.%						
(a)	Z1	66.7	18.8	14.5			-	$\beta - Al_5FeSi$
	Z2	10.4	54.3	-	33.8	1.5	-	$Ti_7Al_5Si_{12}$
	Z1	12.6	55.5	-	30.6	1.2	-	$Ti_7Al_5Si_{12}$
	Z2	11.8	55.7	-	32.5	-	-	$Ti_7Al_5Si_{12}$

Since iron has low solubility in solid $\alpha(Al)$, it tends to combine with other elements to form a variety of intermetallic compounds. The major phases in Al-Si-(Fe) alloys are $\alpha - Al_8Fe_2Si$ (script-like) and $\beta - Al_5FeSi$, or $\alpha - Al_{15}(Fe,Mn)_3Si_2$, or $\pi - Al_8FeMg_3Si_6$ as a dominant phases according to the processing conditions, the Fe percent, and where there are sufficient Mn or Mg, respectively [10,28]. The α and $\pi-$phases can be distinguished by their script-like morphology, unlike the $\beta-$phase which has a platelet morphology. The variant $\alpha - Al_{15}(Fe,Mn)_3Si_2$ can be found, in addition to the typical script-like morphology, in a bulky form [10,29]. This bulky form of $\alpha - Al_{15}(Fe,Mn)_3Si_2$ was dominant in the bulk filler Al-9Si-3Cu, while the script-like form was dominant in the bulk filler Al-13Si before the brazing (Figure 2). Although the addition of Fe to the cast alloys can protect the mold from what is known as die soldering [30], the presence of the $\beta - Al_5FeSi$ phase negatively affects the tensile strength. The $Al_{15}(Fe,Mn)_3Si_2$ phase has less detrimental effects on the mechanical properties [10,25,30]. Due to the low cooling speed in the current brazing process, $\beta - Al_5FeSi$ was dominant in all the brazed joints except when the filler Al-9Si-3Cu was used (Figure 23 for 13/680, Figures 15 and 24 for 13/585, and Figure 25 for 9-3/580 joints, the related EDS analyses results are presented in Tables 3–5). The longest platelet morphology of $\beta - Al_5FeSi$ was observed in the joint 13/680. Whereas in 9-3/580, the bulky $\alpha - Al_{15}(Fe,Mn)_3Si_2$ phase was almost the same before (Figure 2c–d) and after brazing (Figure 25). It seems that the formation of the platelet morphology largely depends on both the cooling speed and the heat provided to the joint when not enough Mn or Mg additions exist in the filler.

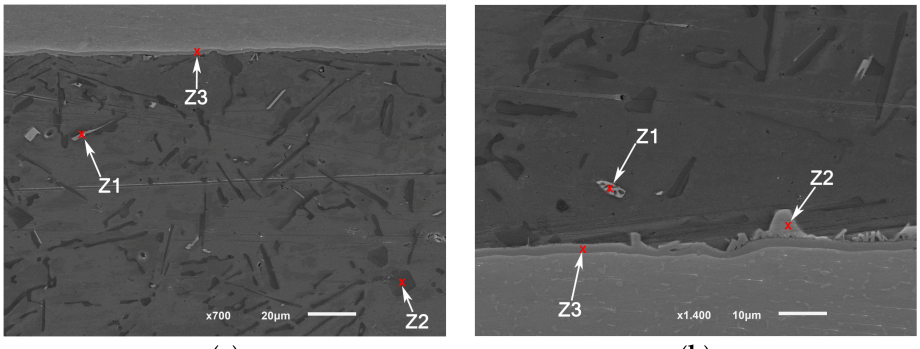

(**a**) (**b**)

Figure 24. SEM images (SEI) of a 13/585 brazed joint: (**a**) The active parent part interface with the filler; (**b**) The passive part interface. EDS analyses results are shown in Table 4.

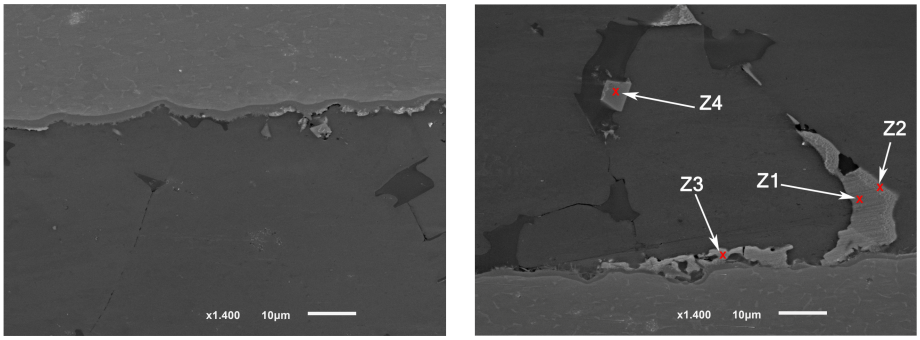

(**a**) (**b**)

Figure 25. SEM images (SEI) of a brazed joint 9-3/580: (**a**) The active parent part interface with the filler; (**b**) the passive part interface. ((b) is taken at relatively farther distance from the middle of the joint). EDS analyses results are shown in Table 5.

Table 4. EDS points analyses for the joint 13/585 presented in Figure 24.

	Element:	Al	Si	Fe	Ti	V	Mn	Estimated Main Phase(s)
		at.%						
(a)	Z1	61.6	25.2	13.3			-	$\beta - Al_5FeSi + Si$
	Z2	1.8	98.2	-	-	-	-	Primary silicon
	Z3	17.3	48.3	-	34.4	-	-	$Ti_7Al_5Si_{12}$
(b)	Z1	85.6	6.2	8.3	-	-	-	$\alpha - Al_8Fe_2Si + Al$
	Z2	72.4	11.6	13.7	0.9	-	1.5	$\alpha - Al_{15}(Mn,Fe)_3Si_2$
	Z3	13.1	50.2	-	36.7	-	-	$Ti_7Al_5Si_{12}$

Table 5. EDS points analyses for the joint 13/680 presented in Figure 25.

	Element:	Al	Si	Fe	Mn	Ni	Cu	Estimated Main Phase(s)
		at.%						
(b)	Z1	70.4	-	-	-	-	29.6	Al_2Cu
	Z2	70.2	-	-	-	-	29.8	
	Z3	71.7		-	-	5.4	22.9	
	Z4	68.2	11.5	15.2	2.3	-	2.9	$\alpha - Al_{15}(Mn,Fe)_3Si_2$+ precipitation of Al_2Cu

Generally, the formation of primary silicon is likely depending on the casting conditions rather than what is expected by the equilibrium phase diagram. According to the phase diagram of Al-Si [31], the primary silicon crystallizes first in the hypereutectic Al-Si alloys, then the left portion of the liquid goes into a eutectic reaction ($L \rightarrow Si_E + \alpha(Al)$). However, the primary silicon particles can be found in the eutectic or even hypoeutectic Al-Si alloys. Si is easy to segregate and forms Si clusters which nucleate and grow at the liquid/solid interface [32]. For a near eutectic composition, the microstructures of the alloy could show a large number of the primary silicon crystals [33]. The amount and size of the primary silicon particles are affected largely by the cooling speed. The suggested growth mechanism was the twin plane re-entrant edge growth mechanism (TPRE) [32] or the dislocation mechanism [33]. Moreover, it was concluded that the distribution of the primary Si particles is nonhomogeneous at any cooling speed [32].

The primary silicon particles were much lower in size and quantity with relatively better distribution in the ultrasonically treated joints using the Al-13Si filler alloy, as with the joints 13/585U and 13/585 at 585 °C when compared with (13/585L) without the ultrasonic treatment (Figures 12a,b, 14, and 15). The samples brazed with Al-3Cu-9Si (9-3/580) were characterized by a thick eutectic silicon (Figure 25) when compared with other joints, and even thicker when compared with the bulk state before the brazing (Figures 2c,d and 25). The USV treatment generally resulted in the reduction of the primary silicon in the joints. Ti could be a contributor in reducing the primary silicon with the assistance of the ultrasonic vibration. It was found that the addition of the Ti reduced the formation of primary silicon [34]. In another study, $TiAl_3$ was found at the surface of the Si phase, which restricted the growth of Si [35].

4. Conclusions

High quality joints were achieved with the assistance of ultrasonic vibration through a precise control of the process parameters, including the temperature, load, and joint gap.

The interaction at the interface between the filler and the base metal can be started by applying an initial compression load, or with USV through pits formation under cavitation. Although the interaction after using a single period of USV was not continuous at the interface, the USV helped to achieve a cleaner joint with better integration and homogeneity. By combining both steps, the initial load and the USV reduced the time needed to produce joints of higher quality that can be further optimized in terms of their mechanical strength.

During the USV, the molten filler is under variable vibration amplitude and acoustic pressure, which creates a limited sputtering and displacement of the filler around the joint. The numerical model that was studied shows the distribution of the vibration amplitude and the developed acoustic pressure vs the gap distance. The acoustic pressure increases by decreasing the joint gap and the temperature, thereby increasing the ability to produce a stronger cavitation cloud. Although the acoustic pressure decreases with the temperature increase, the interaction between the filler and the parent metal has more pronounced effect by increasing the brazing temperature.

The thickness of the intermetallic layer at the joint interface using the filler alloy containing 13% Si was comparable to the total thickness of the intermetallic compounds formed at the interface using 1% of Si if the joint using 13% Si brazed at a temperature close to its liquidus temperature. Unlike the bulky $TiAl_3$ formed in Ti/Al-1Si/Ti joints at a brazing temperature of 680 °C, using the Al-13Si filler produced intermetallic with tiny laminar and scattered morphology at the filler side.

The primary silicon particles were much lower in size and quantity in the ultrasonically brazed samples when compared with samples brazed without the USV. However, the brazing thermal cycle has a dominant effect on the growth of both the eutectic silicon and the needle-like $\beta - Al_5FeSi$ in Al-13Si. A higher brazing temperature of 680 °C resulted in the formation of longer morphology of eutectic silicon and $\beta - Al_5FeSi$ intermetallic.

Author Contributions: Conceptualization, data curation, formal analysis, investigation, methodology, visualization, and writing—original draft: A.M.; resources: A.M. and J.B.; supervision: J.B.; validation: A.M. and J.B. All authors have read and agreed to the published version of the manuscript.

Funding: This work was done with the support of the PEACE II, Erasmus Mundus Lot 2 Project (2013-2443/001-001-EMA2) and the Global Platform for Syrian Students in Portugal.

Data Availability Statement: Not applicable.

Conflicts of Interest: The authors declare no conflict of interest.

References

1. Muhrat, A.; Puga, H.; Barbosa, J. Low-Temperature Brazing of Titanium Using Al-Based Filler Alloys. *Adv. Mater. Sci. Eng.* **2018**, *2018*, 1–16. [CrossRef]
2. Karfoul, M.K.; Muhrat, A.S. *Low Melting Brazing Al-Cu-Ni-Ti Filler Alloys Designed for Joining Titanium under Normal Ambient Air Conditions*; DVS German Welding Society: Aachen, Germany, 2013; Volume 293.

3. Shapiro, A.E.; Flom, Y.A. Brazing of Titanium at Temperatures below 800°C: Review and Prospective Applications. *DVS Ber.* **2007**, *243*, 254.
4. Gemelli, E.; Camargo, N.H.A. Oxidation Kinetics of Commercially Pure Titanium. *Matéria (Rio J.)* **2007**, *12*, 525–531. [CrossRef]
5. Sul, Y. The Significance of the Surface Properties of Oxidized Titanium to the Bone Response: Special Emphasis on Potential Biochemical Bonding of Oxidized Titanium Implant. *Biomaterials* **2003**, *24*, 3893–3907. [CrossRef]
6. Elrefaey, A.; Wojarski, L.; Pfeiffer, J.; Tillmann, W. Preliminary Investigation on Ultrasonic-Assisted Brazing of Titanium and Titanium/Stainless Steel Joints. *Weld. J.* **2013**, *92*, 148–153.
7. Chen, X.; Yan, J.; Gao, F.; Wei, J.; Xu, Z.; Fan, G. Interaction Behaviors at the Interface between Liquid Al-Si and Solid Ti–6Al–4V in Ultrasonic-Assisted Brazing in Air. *Ultrason. Sonochem.* **2013**, *20*, 144–154. [CrossRef]
8. Chen, X.; Yan, J.; Ren, S.; Wei, J.; Wang, Q. Microstructure and Mechanical Properties of Ti–6Al–4V/Al1060 Joints by Ultrasonic-Assisted Brazing in Air. *Mater. Lett.* **2013**, *95*, 197–200. [CrossRef]
9. Chen, X.; Xie, R.; Lai, Z.; Liu, L.; Zou, G.; Yan, J. Ultrasonic-Assisted Brazing of Al–Ti Dissimilar Alloy by a Filler Metal with a Large Semi-Solid Temperature Range. *Mater. Des.* **2016**, *95*, 296–305. [CrossRef]
10. Taylor, J.A. The Effect of Iron in Al-Si Casting Alloys. In Proceedings of the 35th Australian Foundry Institute National Conference, Adeiaide, SA, Australia, 31 October–3 November 2004.
11. Muhrat, A.; Puga, H.; Barbosa, J. Ultrasonic Vibration as a Primary Mixing Tool in Accelerating Aluminum–Copper Alloys Preparation from Their Pure Elements. *Metals* **2019**, *9*, 781. [CrossRef]
12. COMSOL AB. *COMSOL Multiphysics®, v5.4*; COMSOL AB: Stockholm, Sweden, 2018.
13. Åbom, M. *An Introduction to Flow Acoustics*; The Royal Institute of Technology: Stockholm, Sweden, 2006; p. 185. ISSN 1651-7660.
14. COMSOL AB. *COMSOL Multiphysics® Reference Manual, v.5.4*; COMSOL AB: Stockholm, Sweden, 2018.
15. Cheeke, J.D.N. *Fundamentals and Applications of Ultrasonic Waves*; CRC Series in Pure and Applied Physics; CRC Press: Boca Raton, FL, USA, 2002; ISBN 978-0-8493-0130-8.
16. Li, Z.; Xu, Z.; Ma, L.; Wang, S.; Liu, X.; Yan, J. Cavitation at Filler Metal/Substrate Interface during Ultrasonic-Assisted Soldering. Part I: Cavitation Characteristics. *Ultrason. Sonochem.* **2018**, *49*, 249–259. [CrossRef] [PubMed]
17. Bainbridge, I.F.; Taylor, J.A. The Surface Tension of Pure Aluminum and Aluminum Alloys. *Met. Mat Trans A* **2013**, *44*, 3901–3909. [CrossRef]
18. Matsu, K.; Miyazawa, Y.; Nishi, Y.; Ariga, T. Brazing and Interfacial Reaction of Commercially Pure Titanium with Ti-Zr-Based Filler Metals. *Mater. Trans.* **2007**, *48*, 1055–1059. [CrossRef]
19. Ganjeh, E.; Sarkhosh, H. Microstructural, Mechanical and Fractographical Study of Titanium-CP and Ti–6Al–4V Similar Brazing with Ti-Based Filler. *Mater. Sci. Eng. A* **2013**, *559*, 119–129. [CrossRef]
20. Ganjeh, E.; Sarkhosh, H.; Bajgholi, M.E.; Khorsand, H.; Ghaffari, M. Increasing Ti–6Al–4V Brazed Joint Strength Equal to the Base Metal by Ti and Zr Amorphous Filler Alloys. *Mater. Charact.* **2012**, *71*, 31–40. [CrossRef]
21. Chang, C.T.; Du, Y.C.; Shiue, R.K.; Chang, C.S. Infrared Brazing of High-Strength Titanium Alloys by Ti–15Cu–15Ni and Ti–15Cu–25Ni Filler Foils. *Mater. Sci. Eng. A* **2006**, *420*, 155–164. [CrossRef]
22. Du, Y.C.; Shiue, R.K. Infrared Brazing of Ti–6Al–4V Using Two Silver-Based Braze Alloys. *J. Mater. Process. Technol.* **2009**, *209*, 5161–5166. [CrossRef]
23. Ganjeh, E.; Sarkhosh, H.; Khorsand, H.; Sabet, H.; Dehkordi, E.H.; Ghaffari, M. Evaluate of Braze Joint Strength and Microstructure Characterize of Titanium-CP with Ag-Based Filler Alloy. *Mater. Des.* **2012**, *39*, 33–41. [CrossRef]
24. Takemoto, T.; Nakamura, H.; Okamoto, I. Strength of Titanium Joints Brazed with Aluminum Filler Metals. *Transactions JWRI* **1990**, *19*, 45–49.
25. Takemoto, T.; Okamoto, I. Intermetallic Compounds Formed during Brazing of Titanium with Aluminium Filler Metals. *J. Mater. Sci.* **1988**, *23*, 1301–1308. [CrossRef]
26. Xu, L.; Cui, Y.Y.; Hao, Y.L.; Yang, R. Growth of Intermetallic Layer in Multi-Laminated Ti/Al Diffusion Couples. *Mater. Sci. Eng. A* **2006**, *435–436*, 638–647. [CrossRef]
27. Gupta, S.P. Intermetallic Compounds in Diffusion Couples of Ti with an Al–Si Eutectic Alloy. *Materials Characterization* **2002**, *49*, 321–330. [CrossRef]
28. Seifeddine, S.; Svensson, I.L. The Influence of Fe and Mn Content and Cooling Rate on the Microstructure and Mechanical Properties of A380-Die Casting Alloys. *Metallurgical Science and Technology* **2009**, *27*, 10.
29. Dinnis, C.M.; Taylor, J.A.; Dahle, A.K. Porosity Formation and Eutectic Growth in Al-Si-Cu-Mg Alloys Containing Iron and Manganese. In Proceedings of the 9th International Conference on Aluminium Alloys 2004, Brisbane, QLD, Australia, 2–5 August 2004; pp. 1016–1021.
30. Han, Q.; Viswanathan, S. Analysis of the Mechanism of Die Soldering in Aluminum Die Casting. *Met. Mat Trans A* **2003**, *34*, 139–146. [CrossRef]
31. Murray, J.L.; McAlister, A.J. The Al-Si (Aluminum-Silicon) System. *Bull. Alloy Phase Diagr.* **1984**, *5*, 74–84. [CrossRef]
32. Wang, S.; Ma, R.; Wang, Y.; Wang, Y.; Yang, L. Growth Mechanism of Primary Silicon in Cast Hypoeutectic Al-Si Alloys. *Trans. Nonferrous Met. Soc. China* **2012**, *22*, 1264–1269. [CrossRef]
33. Wang, R.-Y.; Lu, W.-H.; Hogan, L.M. Faceted Growth of Silicon Crystals in Al-Si Alloys. *Met. Mat Trans A* **1997**, *28*, 1233–1243. [CrossRef]

34. Kim, J.; Lee, K.; Lee, H.; Lee, T.; Park, H.; Park, H. Effects of Titanium and Boron Additions with Mechanical Stirring on Mechanical Properties in Al-Si Alloys. *Mater. Trans.* **2015**, *56*, 450–453. [CrossRef]
35. Basak, S.; Biswas, P.; Patra, S.; Roy, H.; Mondal, M.K. Effect of TiB2 and Al3Ti on the Microstructure, Mechanical Properties and Fracture Behaviour of near Eutectic Al-12.6Si Alloy. *Int. J. Min. Met. Mater.* **2021**, *28*, 1174–1185. [CrossRef]